Local Polynomial Method Frequency-Response Calculation
for Rotorcraft Applications

Benjamin Fragnière
Research Engineer
German Aerospace Center (DLR)
Braunschweig, Germany

Johannes Wartmann
Research Engineer
German Aerospace Center (DLR)
Braunschweig, Germany

ABSTRACT

Frequency-response function calculation is an essential element in rotorcraft data analysis, especially for system identification, model validation and model analysis. This article analyzes the performance of a recently developed method for the calculation of frequency-response functions, called the local polynomial method (LPM), when applying it to rotorcraft systems. The local polynomial method is presented as an alternative to the methods that are based on segmenting and windowing the data and is particularly effective in reducing the leakage error. The performance of both methods is first compared based on simulated data from linear helicopter models in various conditions. The simulated data allows to separately investigate the influence of: signal-to-noise ratio, signal length, frequency range, type of excitation and input correlation. The conditions under which the local polynomial method is superior to the windowing methods are given. Finally, flight test data are used to validate the results observed in the simulations.

NOTATION

f_s	sampling frequency $(1/s)$
F_{xx}	autospectrum of x
F_{xy}	cross-spectrum of x and y
G	frequency-response function
g_s	Taylor coefficients of G
I_{nu}	identity matrix of dimension n_u
J	cost function $(-)$
k	DFT line
LPM	local polynomial method
LS-Spec	least-squares of spectra method
ML-Amp	maximum-likelihood of amplitude and phase method
m	number of segments
N	number of samples of the signal
n_u	number of inputs
n_{Win}	number of windows
p	roll rate (rad/s)
R	order of the polynomial approximation
RMSE	root mean square error $(-)$
SNR	signal-to-noise ratio $(-)$
T	DFT of the leakage term
t_s	Taylor coefficients of T
T_{Win}	window size (s)
$u(t)$	input signal
$U(k)$	DFT of the input signal
$w(t)$	window function $(-)$
W_i	weighting function
$y(t)$	output signal
$Y(k)$	DFT of the output signal
α, β	curve fitting parameters for the SNR-RMSE equation
δ_x	longitudinal cyclic input $(\%)$
δ_y	lateral cyclic input $(\%)$
ε_r	random error $(-)$
ϕ	phase of the FRF
γ_{xy}	coherence of x and y $(-)$
ω	frequency (rad)
Θ	matrix of unknown parameters

INTRODUCTION

The characterization of a dynamical system from experimental data commonly starts with the calculation of its frequency-response function (FRF). The FRF provides the gain and phase of the output signal as a function of the input signal frequency. In rotorcraft data analysis like in many other research fields, an accurate calculation of the system's FRF is necessary to provide an optimal basis for further evaluation. The FRF can be used as-is for the analysis of the frequency behavior of a system, but it is most often used as an intermediate step for system and parameter identification or for model validation. FRF calculation methods have been used for rotorcraft system identification since the 1980th, see (Refs. 1–3). Over the last decades the applied methods have been enhanced to account for the requirements of rotorcraft environment: time-limited measurements, non-periodic inputs, multiple-input and multiple-output (MIMO) systems, poor signal-to-noise-ratio, etc.

A well-known phenomenon appearing when transforming such finite and non-periodic signals from the time to the frequency domain are leakage errors. In the frame of FRF calculation, leakage can be interpreted as a transient term resulting

from neglecting the input coming before the start of the record and the output coming after the end of the record, (Ref. 4). Leakage yields a biased and thus corrupted estimate of the FRF even in the absence of disturbing noise.

A classical way to reduce leakage is to multiply the signals by a special window before performing the transform into the frequency domain. The window has the task of bringing the initial and final condition of the signal record to the same value (usually zero) while minimizing the spectral impact in the frequency domain. No window is able to totally suppress the leakage error. The shorter the duration of a record is, the higher the level of leakage will be. Therefore the leakage issue will especially be present when segmenting a signal record into several (shorter) sub-records. When FRFs are sought that are valid over a broad range of frequencies, different window sizes are used and combined to form a composite FRF. Therefore FRF calculation methods using windows to reduce leakage errors are called "composite windowing methods" hereafter.

Whereas the usage of windows has been a standard for FRF calculation since the 1980's, a new method, so-called Local Polynomial Method (LPM), was developed at the end of the 2000's (Refs. 5–8). LPM is presented as an alternative to the windowing methods, with better performance due to an improved reduction of the leakage error. Examples of analysis of the LPM performance can be found for various dynamical systems, such as electrical circuits, flexural vibrations of a steel beam, flutter of an aircraft wing or vibrations of an arc bridge (Refs. 7–9).

In this article, the performance of the LPM when applying it to rotorcraft systems is assessed and compared to proven composite windowing methods. For this aim, first simulated data is used to investigate under which circumstances and to which extend the LPM is superior to the composite windowing methods. Finally, flight test data of DLR's research rotorcraft ACT/FHS (Active Control Technology/Flying Helicopter Simulator, a highly modified EC135, see e.g. (Ref. 10) and Figure 1) is used for validation of the simulation results.

Fig. 1: DLR's ACT/FHS research rotorcraft.

FREQUENCY-RESPONSE CALCULATION METHODS

Common frequency-response calculation methods segment the time domain input and output signals using different windows before transforming the time domain signal into the frequency domain. When FRFs are sought that are valid over a broad range of frequencies, composite windowing methods are often applied. These methods work with different segment lengths and calculate the final composite FRF from the results for each segment length though an optimization process. Two investigated implementations of composite windowing methods and the new local polynomial method are described briefly in this section.

Composite Windowing Methods

The overall frequency-response calculation sequence of composite windowing methods is depicted in Figure 2. The first windowing method considered in this paper has been proposed in (Ref. 11) and is used in CIFER®. This method is explained in detail in (Ref. 12) and has been extensively used for rotorcraft system identification: e.g. Bo-105, UH-60, Bell-206, AH-64, SH-2G etc. This method was implemented independently at DLR by (Ref. 13). Therefore, the results of this method are considered to be similar to the CIFER® results, but are not generated with CIFER®.

The second method is presented in (Ref. 14). Both methods are used in DLR's system identification tool FITLAB and have been applied e.g. for model validation in the frequency domain of DLR's research rotorcraft ACT/FHS (Refs. 15,16).

Because the main difference between both methods lies in the way, the composite FRF is calculated from the results for the individual windows, the first method is called "LS-Spec" (Least-Squares of Spectra) and the second method "ML-Amp" (Maximum-Likelihood of Amplitude and Phase) in the following.

Segmenting and Windowing In the first step of frequency-response calculation, the input and output signals are subdivided into m segments and multiplied with a window function $w(t)$ in the time domain. The optimal window size T_{win} to ensure leakage error suppression on one hand and preservation of the information content on the other is large for low frequencies and small for high frequencies. Thus, there is no optimal window setting and different window sizes T_{win} are used consecutively. The results are composed afterward.

LS-Spec uses half-sine windows

$$w(t)_{\text{half−sine}} = \sin\left(\pi\frac{t}{T_{\text{win}}}\right) \tag{1}$$

with a window overlap of 67%. The minimum and maximum window length are chosen based on the frequency range of interest and the guidelines given in (Ref. 12). Generally, five equally distributed windows are used.
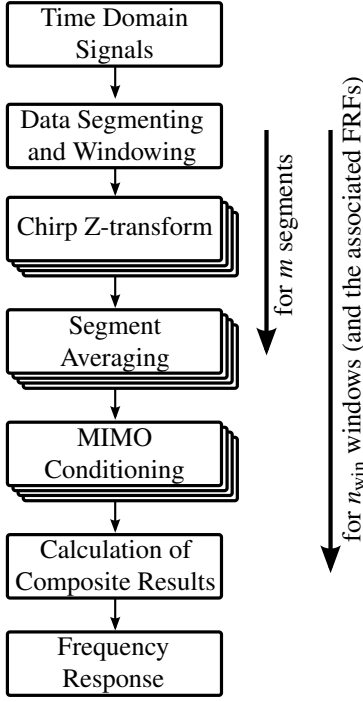
Fig. 2: Frequency-response calculation sequence of the composite windowing methods.

ML-Amp applies the commonly used Hanning window

$$w(t)_{\text{Hanning}} = \frac{1}{2}\left(1 - \cos\left(\frac{2\pi t}{T_{\text{win}}}\right)\right) \qquad (2)$$

with 50% overlap to segment and window the time domain signals. The validity function

$$f_1 \cdot \left(\frac{m}{10}\right)^2 \le f_k \le f_1 \cdot \left(\left(\frac{m}{10}\right)^2 + 14\frac{m}{10} + 1\right) \qquad (3)$$

with $f_1 = \frac{m+1}{2 \cdot N \cdot t_{s_i}}$ describes for any number of segments m which frequencies f_k are in the the frequency range of validity. This function is empirical but provides good results for helicopter response data. Based on the desired frequency range, the validity function gives the minimum and maximum number of segments necessary. All segment numbers between these minimum and maximum values are used.

Chirp Z-transform In the next step, each segment for each window size is transformed from the time into the frequency domain using the Chirp Z-transform (CZT). The CZT is a fast Fourier transform (FFT) that has the advantage, that the desired frequency points can be specified and are not equally distributed on the unit circle.

Segment Averaging The m CZT results for each segment of one window are averaged afterward. The averaged input autospectrum is given by

$$\widehat{F}_{xx}(\omega) = \left(\frac{1}{Um}\right)\sum_{k=1}^{m} F_{xx,k}(\omega) \qquad (4)$$

with the scaling factor U depending on the window function. The output autospectrum $\widehat{F}_{yy}(\omega)$ and cross-spectrum $\widehat{F}_{xy}(\omega)$ are determined in the same way.

MIMO Conditioning For coupled MIMO systems with correlated inputs, the spectra have to be conditioned to reduce the influence of secondary inputs to the selected output. The general solution for the FRF G used by the LS-Spec for multiple inputs is formulated as the matrix equation

$$\widehat{G}(\omega) = \widehat{F}_{xx}^{-1}(\omega)\widehat{F}_{xy}(\omega) \qquad (5)$$

and is then solved for each frequency point ω, (Ref. 17). ML-Amp corrects the spectra iteratively, (Ref. 18).

Calculation of Composite Results The main difference between both methods lies in the way, the composite FRF is calculated from the results for the different window lengths. The LS-Spec method calculates all composite spectra from one cost function, whereas the ML-Amp method calculates the composite amplitudes, phases and coherences separately from the results for the different windows.

For the LS-Spec method, the random error

$$\varepsilon_r = C_\varepsilon \frac{\left(1 - \gamma_{xy}^2\right)^{\frac{1}{2}}}{|\gamma_{xy}|\sqrt{2m}} \qquad (6)$$

(with γ_{xy} the coherence function and C_ε a constant to account for window overlap) is used to calculate the weighting functions W_i for each frequency ω and each window i

$$W_i = \left(\frac{\varepsilon_{r,i}}{\varepsilon_{r,\min}}\right)^{-4}. \qquad (7)$$

Then, the weighted least-squares cost function

$$J(\omega) = \sum_{i}^{n_{\text{Win}}} W_i \left[\left(\frac{\widehat{F}_{xx,c}-\widehat{F}_{xx,i}}{\widehat{F}_{xx}}\right)^2 + \left(\frac{\widehat{F}_{yy,c}-\widehat{F}_{yy,i}}{F_{yy}}\right)^2 \right.$$
$$\left. \left(\frac{\widehat{F}_{xy,c}-\widehat{F}_{xy,i}}{F_{xy}}\right)^2 + 5.0 \left(\frac{\widehat{\gamma}_{xy,c}-\widehat{\gamma}_{xy,i}}{\gamma_{xy}}\right)^2\right] \qquad (8)$$

(with n_{Win} the number of windows) is minimized iteratively for each frequency ω to calculate the composite spectra. Note that the real and imaginary parts of $\widehat{F}_{xy}$ are evaluated separately. Several post processing steps ensure smooth spectra after the optimization. The composite frequency-response and coherence function are determined from the composite spectra.

ML-Amp composes the frequency responses for each segment length by maximizing a log-likelihood cost function. A Cauchy-Lorentz distribution of the weighted difference between the amplitude estimate and the mean amplitude for each frequency point is used in the optimization. The differences are weighted with the amplitude standard deviation

$$\sigma\left(|G(\omega)|\right) = \varepsilon_r(\omega)|G(\omega)| \qquad (9)$$

3

and are only used, if they satisfy the validity function in equation (3). The phase and coherence are optimized in a similar way using the standard deviation

$$\sigma(\varphi(\omega)) = \sigma(\gamma_{xy}(\omega)) = \arcsin(\varepsilon_r(\omega)). \quad (10)$$

Thus, no composite spectra are estimated, but the final frequency-response and the corresponding coherence are determined directly.

Local Polynomial Method
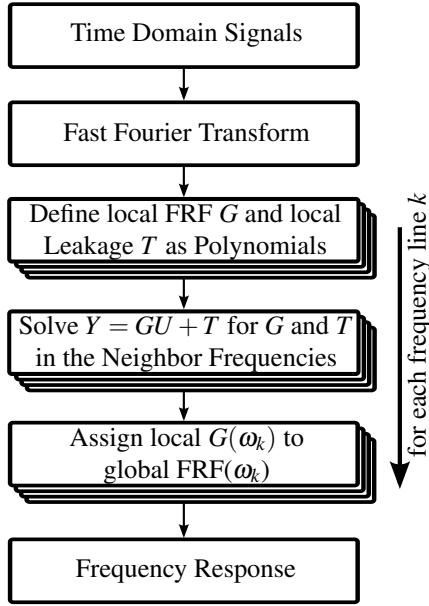
Fig. 3: Frequency-response calculation sequence of the Local Polynomial Method.

An overview of the frequency-response calculation sequence of the Local Polynomial Method (LPM) is depicted in Figure 3. In contrast to the windowing methods, the LPM does not eliminate the leakage term through the application of windows, but it considers the leakage as an unknown function that has to be determined. Hence, the LPM assumes that the discrete Fourier transform (DFT) of the input $u(t)$ and output $y(t)$ measurements

$$U(k) = \frac{1}{\sqrt{N}} \sum_{t=0}^{N-1} u(t) e^{-j2\pi t/N}$$
$$Y(k) = \frac{1}{\sqrt{N}} \sum_{t=0}^{N-1} y(t) e^{-j2\pi kt/N} \quad (11)$$

are linked by the so-called extended transfer function model

$$Y(k) = G(\omega_k)U(k) + T(\omega_k) + V(k) \quad (12)$$

for each DFT line k $(k = 1,...,N)$ of frequency $\omega_k = 2\pi k f_s/N$. Here f_s is the sampling frequency, N the number of samples, $G(\omega_k)$ the FRF of the system, $T(\omega_k)$ the leakage term and $V(k)$ the DFT of the disturbing noise, which is assumed to be a filtered white noise, uncorrelated over the DFT lines k and circular complex distributed.

The estimation of the FRF with the LPM is based on the assumption that the FRF $G(\omega)$ and the leakage $T(\omega)$ are smooth functions of frequency. Therefore, they can be approximated by complex polynomials within a narrow frequency band. The polynomial approximations at frequencies ω_{k+r} $(r = ..., -2, -1, 0, 1, 2, ...)$ of $G(\omega)$ and $T(\omega)$ of the order R and centered around frequency ω_k are given by

$$G(\omega_{k+r}) = G(\omega_k) + \sum_{s=1}^{R} g_s(k)r^s,$$
$$T(\omega_{k+r}) = T(\omega_k) + \sum_{s=1}^{R} t_s(k)r^s, \quad (13)$$

where g_s and t_s are the Taylor coefficients of G and T respectively. R is a parameter of the method that has to be chosen by the user, but is usually set to $R = 2$ in the literature.

Considering equation (12) at frequency $k + r$ and using equation (13) leads to

$$Y(k+r) = \left(G(\omega_k) + \sum_{s=1}^{R} g_s(k)r^s\right) U(k+r)$$
$$+ \left(T(\omega_k) + \sum_{s=1}^{R} t_s(k)r^s\right) + V(k+r) \quad (14)$$
$$= \Theta K(k+r) + V(k+r)$$

where Θ is the matrix of the unknown complex parameters, namely the Taylor coefficients of G and T at frequency k,

$$\Theta = \begin{bmatrix} G(\omega_k) \ g_1(k) \ g_2(k) \ ... \ g_r(k) \ T(\omega_k) \ t_1(k) \ t_2(k) \ ... \ t_r(k) \end{bmatrix}. \quad (15)$$

$K(k+r)$ contains the input data

$$K(k+r) = \begin{bmatrix} K_1(r) \otimes U(k+r) \\ K_1(r) \end{bmatrix} \quad (16)$$

with

$$K_1(r) = \begin{bmatrix} 1 \\ r \\ \vdots \\ r^R \end{bmatrix}$$

Collecting equation (14) for the $2n+1$ neighbours of frequency k $(r = -n, -n+1, ..., n)$ gives the following set of equations

$$Y_n = \Theta K_n + V_n \quad (17)$$

where Y_n, K_n and V_n are matrices with the form

$$Y_n = \begin{bmatrix} Y(k-n) \ Y(k-n+1) \ ... \ Y(k) \ ... \ Y(k+n) \end{bmatrix}. \quad (18)$$

n is a parameter of the method that has to be chosen by the user under the constraint $2n+1 \geq (R+1)(n_u+1)$, with n_u being the number of inputs. The constraint ensures that

equation (17) is an over-determined set of equations for the unknown estimate $\widehat{\Theta}$ that is to be solved in least-square sense

$$\min_{\Theta} \|Y_n - \Theta K_n\| . \tag{19}$$

The choice of the parameter n is a trade-off between an effective noise reduction (n big) and a low interpolation error (n small). In (Ref. 19), a method is described that allows choosing the optimal n at every frequency k. Thus $\widehat{\Theta}$ provides the best fitting complex polynomials for G and T around frequency k. The FRF estimate at k-th frequency is obtained from $\widehat{\Theta}$ using

$$\widehat{G}(\omega_k) = \widehat{\Theta} \begin{bmatrix} I_{n_u} \\ 0 \end{bmatrix} \tag{20}$$

with I_{n_u} being the identity matrix of dimension n_u. The steps above are repeated for every frequency k of the spectrum. Note that special attention has to be paid to the lower and higher edge frequencies of the spectrum. There, the $2n + 1$ neighbouring frequencies cannot be centered around the frequency k, but have to be shifted to the right or to the left respectively.

LPM is available for both SISO and MIMO systems and is described in details in (Ref. 4). It has been shown in (Ref. 8) that using concatenated data leads to a reduced bias and variance error of the FRF estimate. The MIMO algorithm of the LPM can be used unchanged for concatenated data.

COMPARISON OF THE METHODS

In order to systematically compare the performance of the LPM and the composite windowing methods, a set of simulations has first been run using analytical linear helicopter models, whose true FRF is known. The input and output signals from these simulations have been used to calculate an estimate of the FRF through the different methods. The use of analytical models allows comparing the respective errors of the FRF estimates. Two different helicopter models have been used and simulations have been run with varying signal-to-noise ratios, signal lengths, excitation types, noise spectral distributions and correlations between the input signals.

Simulation Models

The first simulation system is the identified Bo-105 helicopter model from (Ref. 11), reduced to the states of pitch and roll rates, longitudinal and lateral flapping angles and two lateral lead-lag canonical states. This model has the advantage to present three distinct FRF profiles along the spectrum: largely constant in the lower frequencies, with a resonance shape at medium frequencies and with a quickly decreasing profile for the higher frequencies. The transfer function from the lateral cyclic δ_y to the roll rate p for this model is shown in a Bode diagram in Figure 4.

The second model used for the simulations is a high-order model of the ACT/FHS at 60 knots with 35 internal states. This model is a result of the identification performed
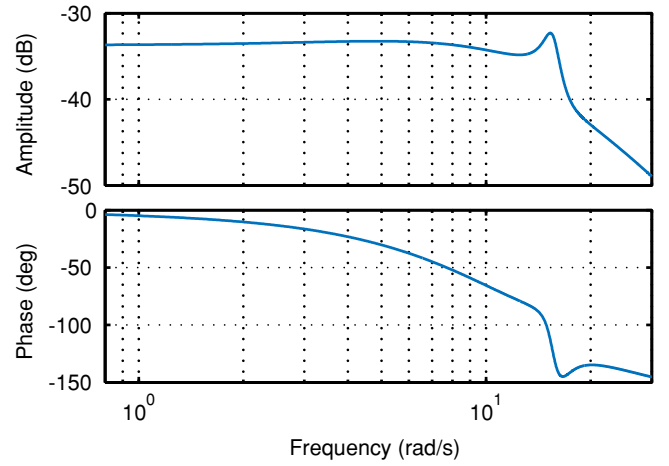
Fig. 4: Transfer function from δ_y to p of the simplified Bo-105 model.

in (Ref. 16) and has been slightly modified to be stable. Its transfer function from δ_y to p is shown in a Bode diagram in Figure 5.
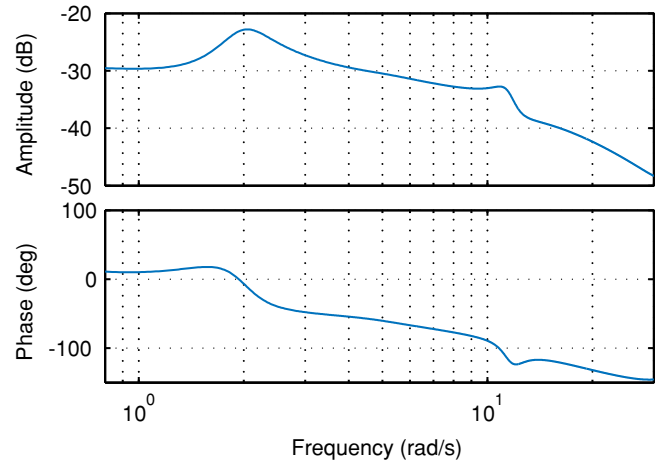
Fig. 5: Transfer function from δ_y to p of the stabilized high-order model of the ACT/FHS.

Signal-to-Noise Ratio

The first set of simulations used for the calculation of a FRF estimate is run with a white noise excitation in one input and no excitation in the others. The output is taken without any disturbing noise. A white noise has been chosen as input signal because this type of excitation permits to have a homogeneous power distribution along the frequency spectrum and is therefore optimal for a generic analysis. The section Type of Excitation below investigates the difference of results between a white noise excitation and a sweep excitation. All simulations performed in this study confirm the theoretical result that the LPM always performs better than the windowing methods in the absence of disturbing noise, (Ref. 6). See Figure 6 for an example of the FRF estimate of the different methods from lateral cyclic δ_y excitations to roll rate p for the ACT/FHS

model. In this example, the simulation duration is 90 seconds with samples collected at 500 Hz. The error depicted in Figure 6 is the relative error defined as

$$\text{Error}(k) = \frac{|\text{FRF}_{\text{estimate}}(k) - \text{FRF}_{\text{true}}(k)|}{|\text{FRF}_{\text{true}}(k)|} \quad (21)$$

for each frequency k of the spectrum.

For cases with added noise, the results observed in the simulations vary considerably. No theoretical quantitative indication is given in the literature that allows to compare the LPM with composite windowing methods in presence of disturbing noise. (Ref. 6) states as a general trend that the covariance of the FRF estimate is smaller for the LPM than for the windowing methods. But the same article reveals that some simulations showed opposite results to this general trend.
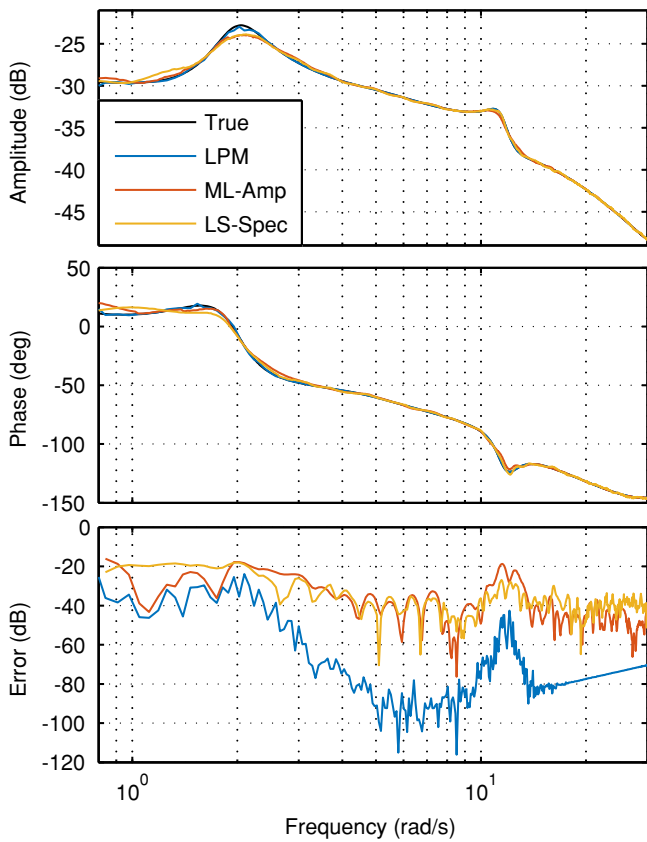
Fig. 6: True and estimated FRF from δ_y to p of the ACT/FHS model in the case without noise.

In order to assess the performance of the different methods with respect to a disturbing noise, simulations have been run with different signal-to-noise ratios (SNR) and the corresponding root mean square (relative) errors (RMSE) of the FRF estimate have been calculated. The results show that for all methods the RMSE is inversely proportional to the square root of the SNR until a threshold value below which the error remains constant, assumed to be the remains of the leakage error. This behavior is modeled with

$$\text{RMSE} = \alpha + \beta / \text{SNR}^{1/2} \quad (22)$$

with α and β being the curve fitting parameters.

Figure 7 shows an example of the RMSE extracted from simulations with different SNR and the fitting curves using equation (22) for both the simplified Bo-105 model and the high order ACT/FHS model. Note that for the the flight tests performed at DLR, SNR ranging from about 20 dB to 40 dB are usually observed.

(a) Simplified Bo-105 model

(b) ACT/FHS model
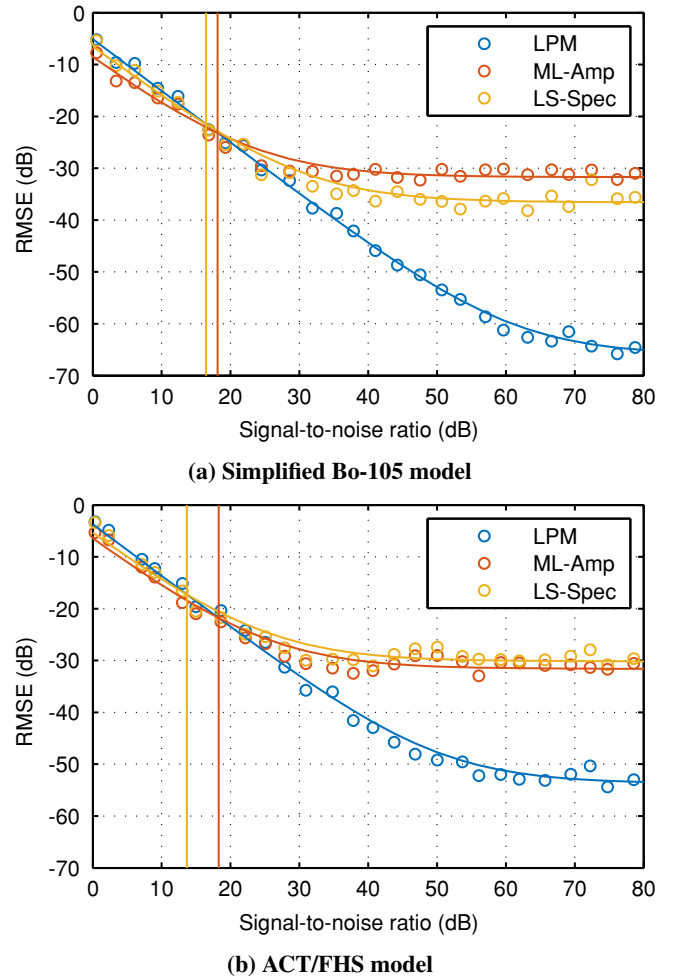
Fig. 7: RMSE of the FRF estimate as a function of SNR for the different methods. The vertical lines indicate the crossover SNR for the two windowing methods.

The following result was observed in most simulations: the RMSE of the LPM is lower than the RMSE of the windowing methods when the SNR is higher than a certain value. Inversely, the RMSE of the LPM is slightly higher than the one of the windowing methods when the SNR is lower than this value. In this paper, this value is called the "crossover SNR" and is used to estimate under which conditions the LPM is superior to the windowing methods (see Figure 7 for an example). A lower crossover SNR means that the LPM performs better than the windowing methods over a wider range of SNR, and vice-versa.

Frequency Range

As seen in the previous section, the superiority of one or the other method depends on the level of noise and on the leakage error present in the data. As both of these characteristics vary with frequency, it is to be expected that the local performance of the methods varies depending on the frequency range considered. In general, every combination of FRF profile, excitation spectrum and noise spectrum gives a different result, but some trends can be given on where the noise level and leakage error will be most present along the spectrum:

a) The lower frequencies commonly have a low SNR. This is due to the fact that not only the sensor noise is considered, but also the equivalent noise caused by non-measured inputs, such as the wind. The wind is an important source of noise in flight test measurements and contains its energy in the lower frequencies. Additionally, low frequency excitations lead to larger amplitude and thus to non-linear helicopter dynamics. Under certain conditions, non-linearities can act as a noise in the FRF calculation (Ref. 7).

b) Both the ML-Amp and the LS-Spec methods use smaller windows for calculating the FRF at the higher frequencies. As the leakage error increases with decreasing number of samples N with $O(N^{-1/2})$, the FRF estimate will be more corrupted by leakage at higher frequencies than at the lower ones, (Ref. 4).

c) The leakage error of the windowing methods is proportional to the second derivative of the true FRF $\frac{d^2 G(\omega)}{d\omega^2}$, (Ref. 4). Therefore, the LPM will be advantageous in the frequency bands where this second derivative is high, typically in resonance areas.

d) The spectral distribution of the leakage along the frequencies is closely linked to the spectral distribution of the FRF. This is due to the fact that the leakage function has by nature the same poles as the FRF of the system (Ref. 4). Therefore, the leakage error is likely to be higher in the frequency bands where the spectral power of the FRF is important, typically in the resonance areas.

In this section, the RMSE of the FRF estimates are calculated separately for three frequency ranges: lower frequencies (1-13 rad/s), resonances area (13-17 rad/s) and higher frequencies (17-30 rad/s), for the simplified model of the Bo-105. Additionally, as the local SNR depends on the distribution of the disturbing noise, a set of filtered white noises with cut-off frequencies ranging from about 1 rad/s to 20 rad/s has been applied. The low-pass shape of the noise accounts for the usual low frequency concentration of the noise present in data coming from a flight test. Note that a high level of noise can also occur locally at higher frequencies due to the vibrations of the rotor and of structural parts, but is not modeled in this simulation.

Regarding the low frequency range, the resulting RMSE curves of the different methods are almost overlapping each other and the curve of the LPM separates only slowly from the other curves. Therefore, in this section the definition of crossover SNR is slightly modified: it is not exactly the SNR at which the curves cross, but the SNR at which the curves separate by 3 dB. For each noise cut-off frequency and each frequency range, this crossover SNR is shown in Figure 8 for the two windowing methods.
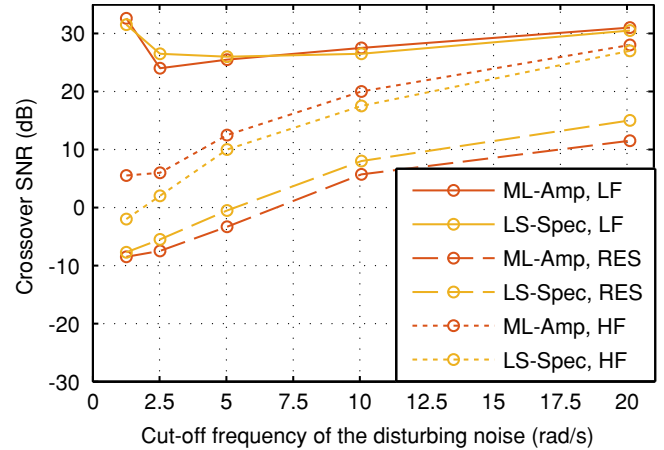
Fig. 8: Crossover SNR for different noise cut-off frequencies and different ranges of the frequency domain, based on the Bo-105 model (LF = low frequencies, RES = resonance, HF = high frequencies).

Considering that the SNR of a good flight test typically has a value between 20 dB and 40 dB, it can be seen that independently of the cut-off frequency the LPM does not perform better than the windowing methods at the lower frequencies, but it always performs better around the resonance area. At the higher frequencies, the superiority of one or the other method highly depends on the cut-off frequency of the disturbing noise.

This analysis has been performed with 60'000 samples, corresponding to a simulation time of 2 minutes. The next sections analyzes the impact of the number of samples on the relative performance.

Signal Length

It is shown in (Ref. 4) that for discrete-time systems, the leakage error disappears with $O(N^{-1/2})$, N being the number of samples. The LPM should consequently be superior to the windowing methods for small numbers of samples. Simulations have been performed with N ranging from 15'000 to 90'000 samples, which corresponds to a simulation time of 30 seconds to 3 minutes. The values of α and β from equation (22) have been calculated separately for the lower frequencies, the resonance area and the higher frequencies of the Bo-105 model and are shown in Figure 9a and Figure 9b.

The interpretation of these two parameters is as follows: α corresponds to the minimum RMSE that the FRF estimate can reach and indicates the performance of the method in high-SNR conditions. It can be seen from Figure 9a that the LPM exhibits a lower value of α than the windowing methods for every number of samples. The difference between the α of the composite windowing methods and the α of the LPM gives an
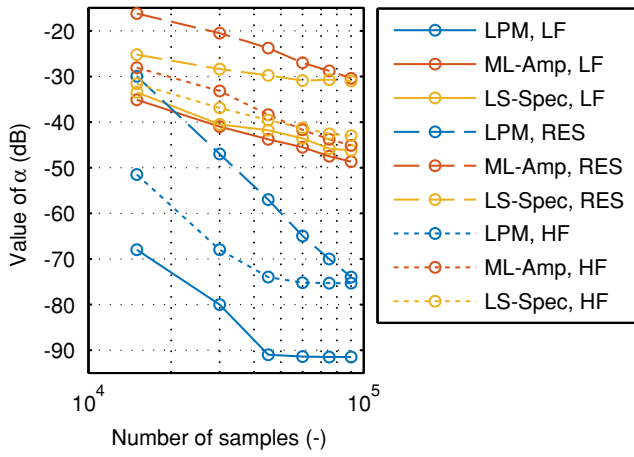
(a) Value of α, the RMSE in the case without noise.
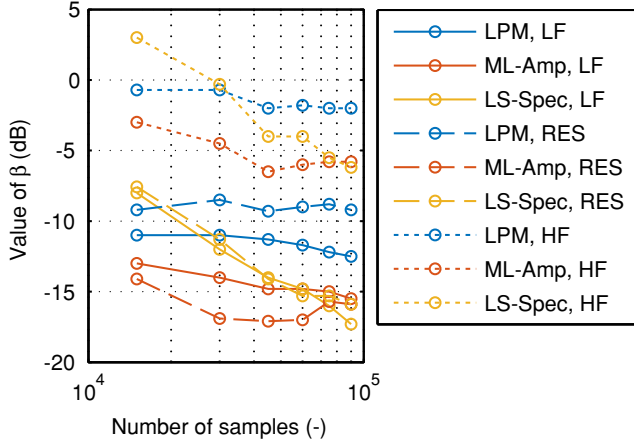
(b) Value of β, the part of the RMSE depending on the SNR.

Fig. 9: Value of α (a) and β (b) from equation (22), for the FRF estimate of the Bo-105 model with varying number of samples (LF = low frequencies, RES = resonance, HF = high frequencies).

idea of the potential benefit of using the LPM rather than the windowing methods. It indicates the maximum improvement that the LPM can reach compared to the windowing methods. For this model, this improvement varies from 3 % (−30 dB) to 10 % (−20 dB) around the resonance, and from <1 % (−48 dB) to 3 % (−30 dB) outside of the resonance area. The same order of possible improvement is obtained for the ACT/FHS model. Additionally, as was expected, the value of α decreases with increasing number of samples (i.e. with decreasing leakage error).

The parameter β represents the dependency of the RMSE on the level of noise and indicates the performance at the lower SNR conditions. The results shown in Figure 9b reveals that if the test duration is longer than one minute (30'000 samples), the value of β is higher for the LPM than for the windowing methods.

Consequently, the LPM is better for low-noise data and worse for noisy data, when compared to the windowing methods. The LPM improvement is best for smaller signal lengths. The crossover SNR for the whole frequency spectrum is

shown in Figure 10 for both the Bo-105 and the ACT/FHS models.

As a side result, it can be observed that with decreasing N the value of α is increasing faster for the ML-Amp method than for the LS-Spec method, and the opposite is true for the value of β. Therefore, comparing just the two windowing methods, LS-Spec should be preferred for low-noise data and ML-Amp for noisy data. Nevertheless, for long measurement times, ML-Amp and LS-Spec methods converge to similar performances.
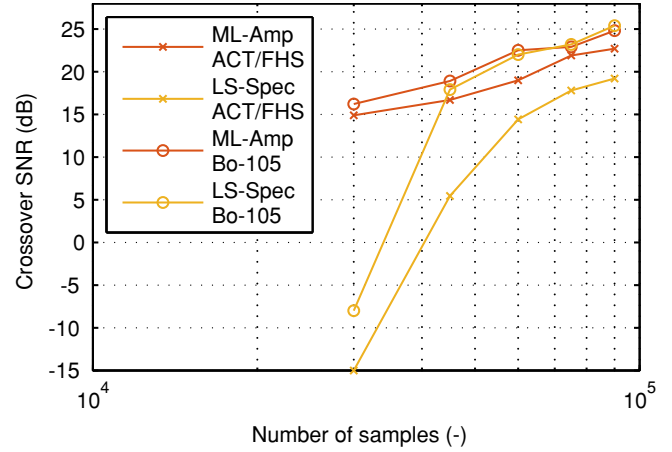
Fig. 10: Crossover SNR for different numbers of data samples on the whole spectrum for the Bo-105 and for the ACT/FHS models.

Type of Excitation

In the previous sections the helicopter models have been excited by white noise to allow a generic analysis. This section aims at verifying that the results obtained in the previous sections with a white noise input are also valid for a sweep input, which is the most common excitation used for system identification. The sweep signals are taken from a flight test campaign of the ACT/FHS (see Figure 12 for an example) and all have a duration of about 100 seconds (50'000 samples), which is an appropriate duration for the frequency range considered in the identification of the ACT/FHS model (0.5-30 rad/s).

Simulations have been run with a sweep excitation and the same analysis was made as before, except that due to the limited frequency bandwidth of the sweep signal the disturbing noise had to be filtered, in order to prevent unrealistically high SNR in the high frequencies. Figure 11 shows the crossover SNR for different noise cut-off frequencies and for different frequency ranges, similar to Figure 8 but with sweep excitation. When comparing Figure 8 and Figure 11, one can see that the results of the LS-Spec methods are quite similar, while the crossover SNR of the ML-Amp method have decreased by 5-10 dB for each situation. However, the conclusions drawn for the white noise excitation are still valid. As all the sweep signals available from flight tests have a similar duration, a variation of the signal duration could not be performed. How-

ever, when compared to the values of α with white noise excitation at 50'000 samples (Figure 9a), the results with sweep excitation are similar for LS-Spec but deteriorate by 3-8 dB for ML-Amp. The LPM performance got worse by 5-10 dB but is still much better than both windowing methods.
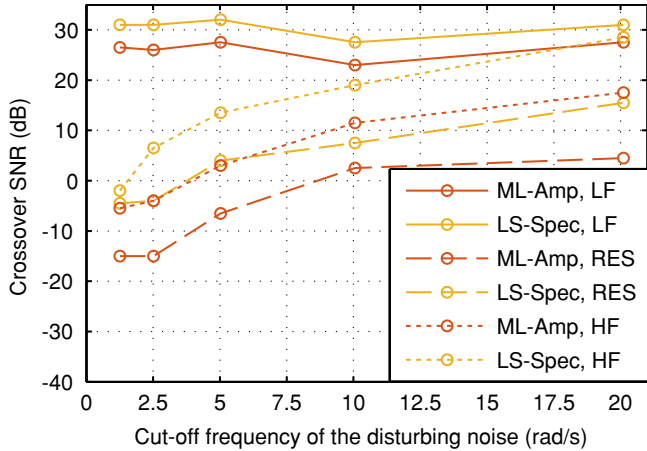
Fig. 11: Crossover SNR for different noise cut-off frequencies and different ranges of the frequency domain, with a sweep excitation and based on the Bo-105 model (LF = low frequencies, RES = resonance, HF = high frequencies).

This difference of performance between white noise excitation and sweep excitation can be explained by a different leakage error in the data. Additionally, as can be seen on Figure 9a, the dependency of α on a variation of number of samples (and thus on a variation of leakage error) is very little for LS-Spec, but is more important for ML-Amp and for LPM. This can explain why α depends on the excitation type for ML-Amp and for LPM but not for LS-Spec.

Input Correlation

When a MISO or MIMO system is excited simultaneously in several axes and when these excitations are correlated, a MIMO conditioning step has to be added in the FRF calculation through the windowing methods, as mentioned in the previous section. This conditioning is required to free the cross-spectra from the influence of the off-axis excitations. The LPM does not proceed through the calculation of the cross-spectra and takes all the input axes into account for the calculation of the FRF estimate. Therefore, it does not require a conditioning step. As the LPM and the windowing methods deal with the issue of input correlation through a different approach, a comparison of the performances under correlated data is performed in this section. To do so, the lateral cyclic δ_y and longitudinal cyclic δ_x are excited simultaneously with

$$\delta_y = S_1 \tag{23}$$
$$\delta_x = \lambda \cdot \delta_y + (1-\lambda) \cdot S_2.$$

where S_1 and S_2 are manual excitations signals taken from a flight test; they are represented in Figure 12. δ_y is a sweep signal and δ_x are the small corrections made by the pilot to keep

the helicopter in the trim attitude. Simulations are run with different values of λ, leading to different levels of correlation.
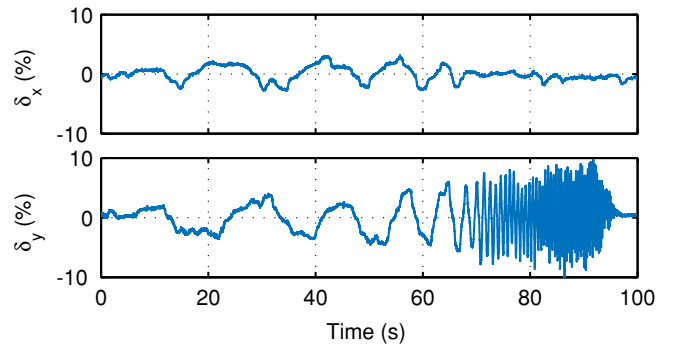
Fig. 12: Manually performed sweep excitation in δ_y and manual trim corrections in δ_x.

The resulting values of α and β as a function of correlation are shown in Figure 13. As expected, the two parameters increase with the correlation level but regarding α the loss of performance is much more important for the windowing methods than for the LPM. As previously said, α represents the maximum improvement that the LPM can achieve compared to the windowing methods. As can be seen in Figure 13a, α can considerably exceed the 10% (-20 dB) mentioned in the section Signal Length, when the correlation level is high.

Figure 14 shows the evolution of the crossover SNR with the input correlation level. One can see that the crossover SNR stays at low SNR level (<15 dB) under all conditions.

VALIDATION WITH FLIGHT TEST DATA

To validate the conclusions drawn in the previous section, the LPM and the composite windowing methods have finally been applied to flight test data. The data used in this section comes from the ACT/FHS system identification campaign performed in 2009 at the DLR. It consists of a series of manual sweep excitations independently in each axis, with only small corrective inputs in the other axes to maintain the helicopter trim (see Figure 12).

The FRF from the lateral cyclic δ_y to the roll rate p is shown in Figure 15 at the last page for the three methods. Figure 16 provides a zoom-in view of the FRF amplitude on the lower frequencies, around the resonance and on the higher frequencies. Additionally, in order to show the consistency between the simulation results and the flight test results, the FRFs obtained with a simulation of the ACT/FHS model excited by the same sweep signal are shown in Figure 17 and Figure 18 for comparison. One can see that the simulation data gives similar results to the flight test results and that the outcome corresponds to the trends described in the previous section. At the low frequencies the FRF estimate of the LPM does not seem to provide better results than the windowing methods. The resonance appears to be more precisely captured by the LPM than by the windowing methods; the latter
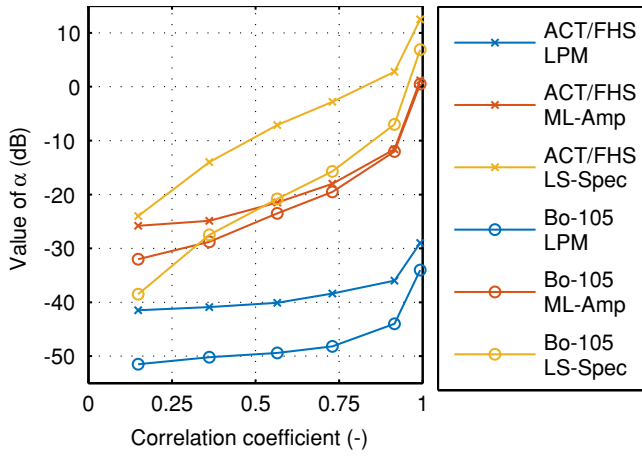
(a) Value of α, the RMSE in the case without noise.
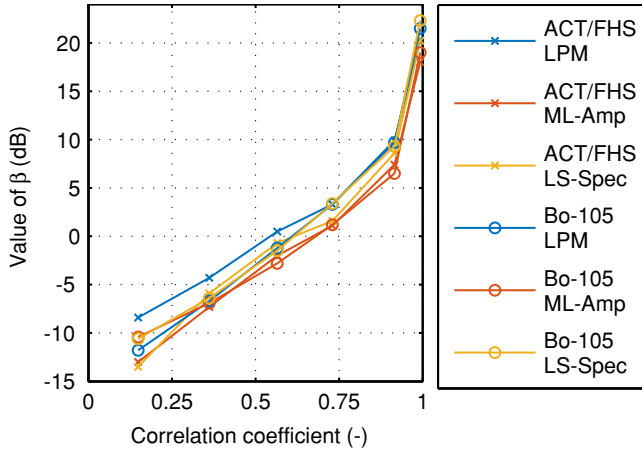
(b) Value of β, the part of the RMSE depending on the SNR.

Fig. 13: Value of α (a) and β (b) from equation (22), for the FRF estimate of the Bo-105 and ACT/FHS models, when excited with a sweep signal, with varying level of correlation.

tend to smooth the peak of the resonance. At high frequencies the estimate of the LPM gives a straight result, while the other estimates oscillate slightly around the true FRF.

No flight test data with a high level of input correlation was available, therefore the superior performance of the LPM for correlated inputs could not be validated in flight.

CONCLUSIONS

In this paper, two variants of the composite windowing method traditionally used for estimating the frequency-response functions (FRF) of rotorcraft systems have been presented, as well as the recently developed Local Polynomial Method (LPM), whose utilization on rotorcraft systems does not appear in the literature, to the author's knowledge. The performance of the LPM has been assessed against the other methods, based on data coming from simulations of linear models of two helicopters. Simulations have been made in different configurations (signal-to-noise ratio (SNR), signal length, frequency range, type of excitation and input correlation) and the errors of the FRF estimates have been compared.
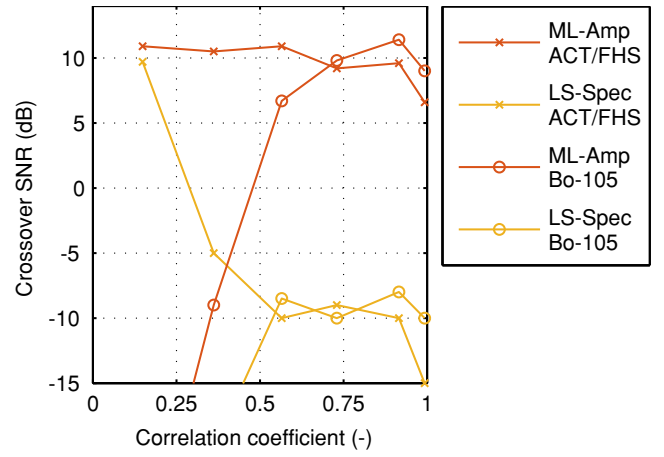
Fig. 14: Crossover SNR for the Bo-105 and ACT/FHS models, when excited with a sweep signal, with varying level of correlation.

Finally, data from a flight test of DLR's ACT/FHS research helicopter has shown consistency with the conclusions drawn from the simulations.

The LPM is not as a whole better or worse than the windowing methods. The LPM is much more effective to counter the leakage effect but rather less effective to counter a disturbing noise. Therefore, in all cases treated here, above a certain threshold of SNR ratio, the LPM always performs better than the other methods and below this threshold, it performs rather worse. The value of this crossover SNR is an indication of the superiority of one or the other method. The following dependencies have been observed:

- The LPM performs better for low-noise data (high SNR).
- The LPM is clearly superior around resonance areas (or in general when the shape of the FRF varies) and performs better at the higher frequencies than at the lower ones.
- The superiority of the LPM is most important for short measurement times (small amounts of samples).
- In the MISO/MIMO case, the LPM is much less affected by a correlation between the input signals.

It is important to note that when the LPM becomes superior, the performance of the other methods is already quite good. In the simulations made in this article, the LPM gave an improvement of up to 10% around the resonances and up to 3% outside of the resonances. Therefore the advantage of using the LPM is rather to fine tune FRF estimates, rather than to improve very noisy FRF estimates. However, when several axes are excited simultaneously, this improvement can greatly exceed the 10% if the inputs are correlated. It is also interesting to note that the LPM captures resonances more precisely, which can be desirable for the calculation of the parametric transfer function. As the windowing methods usually smooth the peaks, they overestimate the damping ratios.

Author contact:
Benjamin Fragnière, benjamin.fragniere@dlr.de
Johannes Wartmann, johannes.wartmann@dlr.de

REFERENCES

[1]Tischler, M. B., Leung, J., and Dugan, D., "Frequency-Domain Identification of XV-15 Tilt-Rotor Aircraft Dynamics," AIAA 2nd Flight Testing Conference, Las Vegas, Nevada, USA, November 1983.
doi: 10.2514/6.1983-2695

[2]Tischler, M. B., Leung, J. G. M., and Dugan, D. C., "Identification and Verification of Frequency-Domain Models for XV-15 Tilt-Rotor Aircraft Dynamics in Cruising Flight," *AIAA Journal of Guidance, Control, and Dynamics*, Vol. 9, (4), July 1986, pp. 446–453.
doi: 10.2514/3.20131

[3]Tischler, M. B. and Kaletka, J., "Modeling XV-15 Tilt-Rotor Aircraft Dynamics by Frequency and Time-Domain Identification Techniques," AGARD FMP Symposium on Rotorcraft Design and Operations, 1987.

[4]Pintelon, R. and Schoukens, J., *System Identification: A Frequency Domain Approach*, John Wiley & Sons, Inc., second edition, 2012.

[5]Schoukens, J., Rolain, Y., and Pintelon, R., "Leakage Reduction in Frequency-Response Function Measurements," *IEEE Transactions on Instrumentation and Measurement*, Vol. 55, (6), December 2006, pp. 2286–2291.
doi: 10.1109/TIM.2006.887034

[6]Pintelon, R., Schoukens, J., Vandersteen, G., and Barbé, K., "Estimation of nonparametric noise and FRF models for multivariable systems—Part I: Theory," *Mechanical Systems and Signal Processing*, Vol. 24, (3), April 2010, pp. 573–595.
doi: 10.1016/j.ymssp.2009.08.009

[7]Pintelon, R., Schoukens, J., Vandersteen, G., and Barbé, K., "Estimation of nonparametric noise and FRF models for multivariable systems—Part II: Extensions, applications," *Mechanical Systems and Signal Processing*, Vol. 24, (3), April 2010, pp. 596–616.
doi: 10.1016/j.ymssp.2009.08.010

[8]Schoukens, J., Vandersteen, G., Rolain, Y., and Pintelon, R., "Frequency Response Function Measurements Using Concatenated Subrecords With Arbitrary Length," *IEEE Transactions on Instrumentation and Measurement*, Vol. 61, (10), October 2012, pp. 2682–2688.
doi: 10.1109/TIM.2012.2196400

[9]Schoukens, J., Vandersteen, G., Barbé, K., and Pintelon, R., "Nonparametric Preprocessing in System Identification: a Powerful Tool," *European Journal of Control*, Vol. 15, (3-4), 2009, pp. 260–274.

[10]Kaletka, J., Kurscheid, H., and Butter, U., "FHS, the New Research Helicopter: Ready for Service," *Aerospace Science and Technology*, Vol. 9, (5), July 2005, pp. 456–467.

[11]Tischler, M. B. and Cauffman, M. G., "Frequency-Response Method for Rotorcraft System Identification: Flight Applications to BO 105 Coupled Rotor/Fuselage Dynamics," *Journal of the American Helicopter Society*, Vol. 37, (3), 1992, pp. 3–17.

[12]Tischler, M. B. and Remple, R. K., *Aircraft and Rotorcraft System Identification: Engineering Methods with Flight-Test Examples*, American Institute of Aeronautics and Astronautics, Inc., Reston, Virginia, USA, second edition, 2012.

[13]Seher-Weiß, S., "Vergleich zweier Verfahren zur Frequenzgangerzeugung," Technical Report IB 111-2014/54, Institut für Flugsystemtechnik, DLR, Braunschweig, Germany, June 2012.

[14]Ockier, C. J., "The Art of Frequency Response Calculation," Technical Report IB 111-97/07, Institut für Flugmechanik, DLR, Braunschweig, Germany, February 1997.

[15]Seher-Weiß, S. and von Grünhagen, W., "EC135 System Identification for Model Following Control and Turbulence Modeling," *Proceedings of the 1st CEAS European Air and Space Conference 2007*, 2007, pp. 2439–2447.

[16]Wartmann, J. and Seher-Weiß, S., "Application of the Predictor-Based Subspace Identification Method to Rotorcraft System Identification," 39th European Rotorcraft Forum, Moscow, Russia, 2013.

[17]Ottnes, R. K. and Enochson, L., *Applied Time Series Analysis, Vol. 1: Basic Techniques*, Vol. 1, John Wiley & Sons, Inc., New York, USA, 1978.

[18]Sridhar, J. K. and Wulff, G., "Application of Multiple-Input/Single-Output Analysis Procedures to Flight Test Data," *Journal of Guidance, Control, and Dynamics*, Vol. 14, (3), May 1991, pp. 645–651.
doi: 10.2514/3.20686

[19]Thummala, P. and Schoukens, J., "Estimation of the FRF Through the Improved Local Bandwidth Selection in the Local Polynomial Method," *IEEE Transactions on Instrumentation and Measurement*, Vol. 61, (10), October 2012, pp. 2833–2843.
doi: 10.1109/TIM.2012.2196393
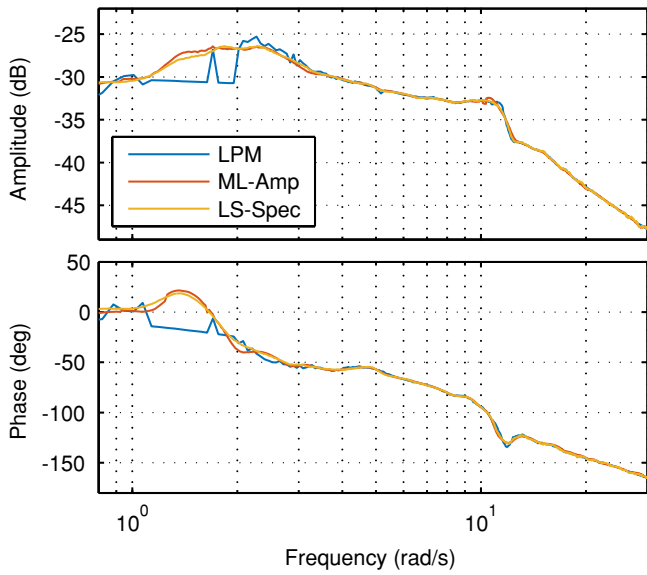
Fig. 15: Estimate of the ACT/FHS FRF from δ_y to p, based on flight test data.
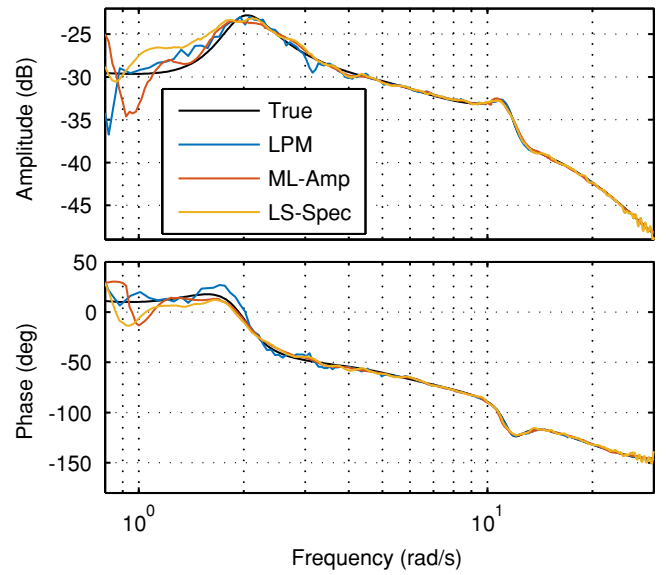
Fig. 17: Estimate of the ACT/FHS FRF from δ_y to p, based on simulation data.
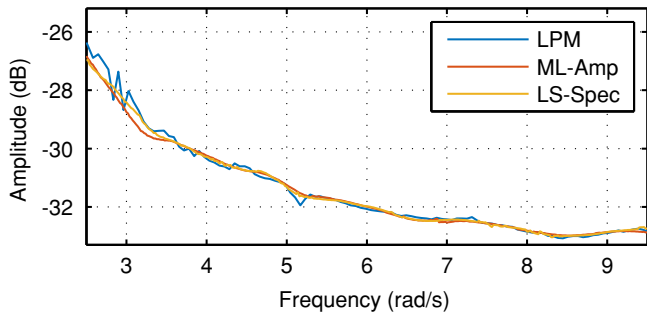
(a) Low frequencies

(a) Low frequencies
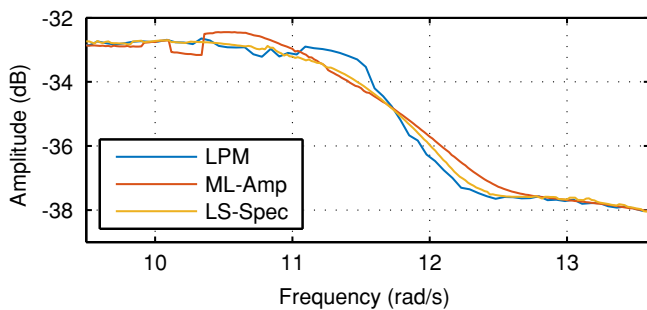
(b) Resonance area

(b) Resonance area
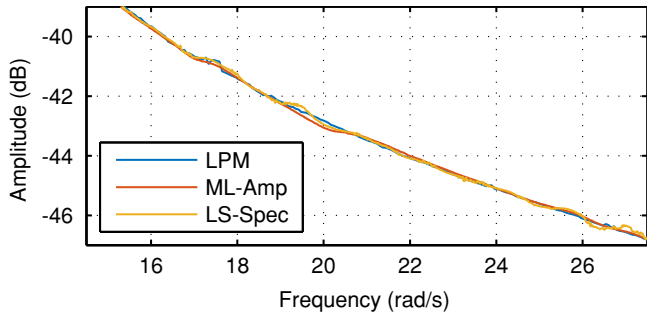
(c) High frequencies

(c) High frequencies

Fig. 16: Zooms on the FRF Estimate based on flight test data.
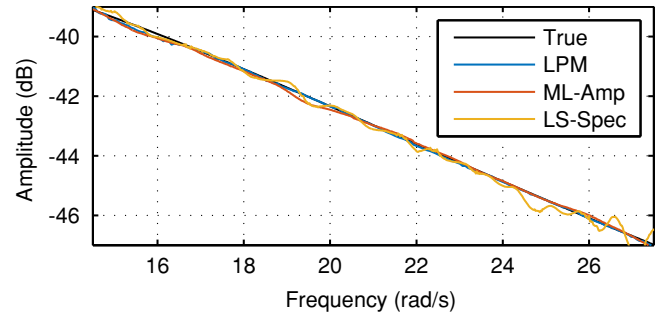
Fig. 18: Zooms on the FRF Estimate based on simulation data.